Distributions of secondary particles in proton and carbon-ion therapy: a comparison between GATE/Geant4 and FLUKA Monte Carlo codes

Distributions of secondary particles in proton and carbon-ion therapy: a comparison between GATE/Geant4 and FLUKA Monte Carlo codes

C Robert[1], **G Dedes**[2], **G Battistoni**[3], **T T Böhlen**[4], **I Buvat**[1], **F Cerutti**[4],
M P W Chin[4], **A Ferrari**[4], **P Gueth**[5,6], **C Kurz**[7], **L Lestand**[8],
A Mairani[9], **G Montarou**[8], **R Nicolini**[3], **P G Ortega**[4,10], **K Parodi**[7],
Y Prezado[1], **P R Sala**[3], **D Sarrut**[5,6] **and E Testa**[2]

[1] IMNC—UMR 8165 CNRS, Universités Paris 7 et Paris 11, Bât 440, F-91 406 Orsay, France
[2] Institut de Physique Nucléaire de Lyon, Université de Lyon, F-69003 Lyon, Université Lyon 1 and IN2P3/CNRS, UMR 5822, F-69622 Villeurbanne, France
[3] INFN, Sezione di Milano via Celoria 16, I-20133 Milano, Italy
[4] European Organization for Nuclear Research CERN, CH-1211, Geneva 23, Switzerland
[5] Creatis, CNRS UMR 5220, F-69622 Villeurbanne, France
[6] Centre de Lutte Contre le Cancer Léon Bérard, F-69373 Lyon, France
[7] Heidelberg Ion-Beam Therapy Center (HIT) and Department of Radiation Oncology, Heidelberg, Germany
[8] Laboratoire de Physique Corpusculaire, 24 avenue des Landais, F-63177 Aubière Cedex, France
[9] Unità di Fisica Medica, Fondazione CNAO, I-27100 Pavia, Italy
[10] Instituto de Fisica Corpuscular (IFIC), CSIC/Universidad de Valencia, E-46071 Valencia, Spain

E-mail: robert@imnc.in2p3.fr

Abstract

Monte Carlo simulations play a crucial role for *in-vivo* treatment monitoring based on PET and prompt gamma imaging in proton and carbon-ion therapies. The accuracy of the nuclear fragmentation models implemented in these codes might affect the quality of the treatment verification. In this paper, we investigate the nuclear models implemented in GATE/Geant4 and FLUKA by comparing the angular and energy distributions of secondary particles exiting a homogeneous target of PMMA. Comparison results were restricted to fragmentation of ^{16}O and ^{12}C. Despite the very simple target and set-up, substantial discrepancies were observed between the two codes. For instance, the number of high energy (>1 MeV) prompt gammas exiting the target was about twice as large with GATE/Geant4 than with FLUKA both for proton and carbon ion beams. Such differences were not observed for the predicted annihilation photon production yields, for which ratios of 1.09 and 1.20 were obtained between GATE and FLUKA for the proton beam and the carbon ion beam, respectively. For neutrons and protons, discrepancies from 14% (exiting

protons–carbon ion beam) to 57% (exiting neutrons–proton beam) have been identified in production yields as well as in the energy spectra for neutrons.

(Some figures may appear in colour only in the online journal)

1. Introduction

Monte Carlo (MC) particle transport methods are increasingly used in medical physics, in particular for the development of innovative techniques for proton and carbon ion therapies. Popular MC packages in this field are Geant4 (Agostinelli *et al* 2003), on which the GATE package (Jan *et al* 2011) is based, FLUKA (Ferrari *et al* 2005, Battistoni *et al* 2007), PHITS (Nose *et al* 2005) or MCNPX (LANL 2008). These codes are increasingly employed to validate the analytical simulation tools used to calculate treatment plans (Paganetti *et al* 2004, Newhauser *et al* 2007, Parodi *et al* 2012, Grevillot *et al* 2012). For such applications, the accuracy of the code is of foremost importance as it might ultimately impact the quality of the treatment plan. MC simulations have also proved to be helpful for *in-vivo* treatment verification based on positron emission tomography (PET) (Parodi *et al* 2002, 2005, Pshenichnov *et al* 2006, Knopf *et al* 2008). Indeed, inaccuracies in the positioning of the patient or anatomical modifications can be detected using PET acquisitions of the annihilation photons resulting from the nuclear reactions undergone by incident ions (Parodi *et al* 2007b). The method consists in comparing the spatial distribution of the annihilation photons predicted by MC simulations based on the treatment plan with the actual PET image. The analysis of any mismatch between the MC simulated image and the PET image makes it possible to detect errors in dose delivery due to patient mispositioning, organ motion or organ deformation. This dose-delivery verification strategy, however, relies heavily on the accuracy of the nuclear fragmentation models implemented in the codes for the specific products used for monitoring.

The GEANT4 code was originally developed for applications in high energy physics. In that energy range, some experimental validations of the hadronic physics integrated in the code have been reported (Geant4-Website 2012a). Conversely, the FLUKA code has been developed and successfully applied both in the high and the low energy ranges. Extensive validations of the hadronic physics against thin target experimental data have been published (Ferrari and Sala 1998, 2002, Battistoni *et al* 2007, Rinaldi *et al* 2011). In the framework of dose calculations in hadrontherapy, the aforementioned codes were also compared with experimental data. For protons, Grévillot *et al* (2010), Koch *et al* (2008) and Parodi *et al* (2007a) showed a good agreement between simulated and experimental depth dose profiles with differences in range smaller than 1 mm. However, some disagreements were observed in the distal fall-off regions with maximum discrepancies of 5% observed between the distal dose predicted by FLUKA and experimental results (Parodi *et al* 2007a). When comparing lateral dose profiles obtained with Geant4 to experimental data, discrepancies up to 20% in the beam widening (FWHM) were observed (Grevillot *et al* 2010). These discrepancies highlighted the need for improving the multi-scattering models of Geant4 (Grévillot *et al* 2010). For carbon ions, available data are scarce (Pshenichnov *et al* 2006, Sommerer *et al* 2006, Lechner *et al* 2010). Comparisons between simulated and experimental data are however promising and suggest that current Geant4 and FLUKA codes correctly reproduce the fragmentation tails beyond the Bragg peak (Sommerer *et al* 2006, Böhlen *et al* 2010, Lechner *et al* 2010, Mairani *et al* 2010). Regarding the lateral beam widening, a good accuracy of FLUKA simulations has been reported in Mairani *et al* (2010).

The accuracy of the internal nuclear models plays an even more important role in the framework of nuclear imaging for hadrontherapy monitoring. However, experimental data

regarding the production of secondary particles are scarce in this context (Parodi *et al* 2002, Gunzert-Marx *et al* 2004, 2008, Haettner *et al* 2006, Polf *et al* 2009, Testa *et al* 2009).

Regarding $\beta+$ production, comparison of FLUKA simulations based on previous versions of the MC internal models to experimental data in proton therapy or carbon ion therapy can be found in Parodi *et al* (2002, 2005), Sommerer (2007) and Sommerer *et al* (2009). Much improved results for protons can be obtained with the present FLUKA models, as demonstrated in this study. The carbon results also profit from the many developments in the Boltzmann master equation (BME) model implemented since Sommerer (2007). Similar studies were carried out in Pshenichnov *et al* (2006) using the Geant4 software. In Parodi *et al* (2002), (2005) and Espana *et al* (2011), a method consisting in convolving the energetic proton fluence with experimental cross-sections was used instead of entirely relying on the MC internal model of nuclear fragmentation. This method, which gives encouraging results in the protontherapy context, can however, not be used in carbon ion therapy today, because of the lack of appropriate experimental cross-section values. Recently, Seravalli *et al* (2012) compared the $\beta+$ emitter productions in depth of three MC codes (GATE/Geant4, MCNPX and PHITS) in homogeneous media in proton therapy. The study shows that for protons the internal models of these three MC codes do not accurately reproduce the spatial distribution of the main $\beta+$ emitters (^{11}C, $^{15}0$).

In the last six years, methods of range verification based on imaging of prompt gammas exiting from the patient have been explored (Min *et al* 2006, Polf *et al* 2009, Testa *et al* 2009, Moteabbed *et al* 2011, Bom *et al* 2012). Collimated gamma camera (Polf *et al* 2009, Testa *et al* 2009, Bom *et al* 2012, Smeets *et al* 2012) as well as Compton camera prototypes (Frandes *et al* 2010, Richard *et al* 2011, Kim *et al* 2012) have been developed or are under construction. Compared to PET imaging, prompt gamma imaging is characterized by higher numbers of emissions (Moteabbed *et al* 2011). Comparisons between experimental data and Geant4 simulations have been performed. They showed that the simulated spectra contained all the characteristic emission lines presented in the measured spectra with proton beams. For carbon ions, initial results reported a 12 times overestimation of the prompt gamma yields (deposited energy higher than 2 MeV, 90° angle with respect to the beam direction, 1.5 ns time-of-flight window) for Geant4 9.1 simulations (Le Foulher *et al* 2010). Results obtained with the Geant4 9.4 version (ENVISION deliverable 2012) are in better agreement with experimental data since the prompt gamma yield is overestimated by a factor of 2. On the other hand, simulations of the same data with FLUKA have steadily provided an overall agreement within 10–15% (Böhlen *et al* 2013).

Comprehensive experimental data regarding the production of secondary particles are missing in ion-beam therapy. When experimental data are lacking, a useful insight into the consistency of MC models can be obtained by comparing the prediction of different models implemented in the codes. In this work, we studied the consistency of depth dose profiles and secondary particle productions as predicted by two MC simulation codes used in the context of hadrontherapy, namely FLUKA and GATE/Geant4. Angular and energy distributions of particles resulting from nuclear interactions of primary protons and carbon ions in a homogeneous PMMA (PolyMethyl MethAcrylate*)* target were compared. The objective was twofold. First, it aimed at identifying potential inconsistencies in the results provided by the two codes to determine the models and model components requiring specific attention and additional validation for a sound use of MC simulations in the context of range verification. Differences smaller than 1% of the incident particle range are desirable for dosimetry applications. For imaging purposes, differences up to 20–30% will be acceptable for prototype dimensioning. A better agreement (differences smaller than 10%) will be necessary for a clinical imaging-based dose monitoring. As a second objective, this study describes a

simple set-up with associated results that could be further referred to for validation of new versions of these two codes or for analysis of the results provided by other codes. This paper is organized as follows. Section 2.1 gives details on the simulation parameters used for each MC code. Sections 2.2, 2.3 and 2.4 describe, respectively, the common set-up, the scored quantities and the studied observables. Results are given in section 3 and then discussed in section 4.

2. Material and methods

Two MC codes, GATE/Geant4 and FLUKA, were employed in this work. Specific details of these codes are described in section 2.1 Special attention was paid on setting identical simulation parameters in the two codes, such as particle transport thresholds and production cuts. The simulated geometries are described in section 2.2 and the scored quantities as well as the observables of interest in our study are presented in sections 2.3 and 2.4.

2.1. GATE and FLUKA MC simulation codes

2.1.1. GATE. GATE version 6 (GATE-Website 2012) is an opensource MC simulation application enabling the modeling of emission tomography, transmission tomography and radiation therapy. GATE is based on the Geant4 toolbox (Geant4-Website 2012b). In this work, GATE version 6.1, based on Geant4 version 9.4, was used. As recommended by the Geant4 Electromagnetic Standard working group, the Opt3 electromagnetic standard package parameters were selected. A fine sampling of the stopping power and cross-section tables (20 bins/decade) was used for improved accuracy. In Geant4, production thresholds expressed in range can be tuned to optimize the computation times. Default values (1 mm) were used for all particles except for electrons for which the production thresholds were set to 12.7 cm and 0.114 mm in air and PMMA respectively. These values were consistent with the δ-ray production threshold (100 keV) which was adopted in the FLUKA simulations. Table 1 describes the hadronic physics list used in the GATE/Geant4 simulations.

The binary cascade (BiC) model (Pshenichnov *et al* 2006, Seravalli *et al* 2012) was applied to protons and neutrons except at low energies where the high precision G4NeutronHP package was used for neutrons. The BiC model was employed without internal calls to the precompound model (so-called 'modified BiC' hereafter) for all particles (Seravalli *et al* 2012). The quantum molecular dynamics (QMD) model recommended by Böhlen *et al* (2010) was activated for all ions (ions heavier than alpha particles, so-called 'generic ions', deuterons, tritons, ^{3}He and alpha). To describe elastic interactions, the HadronElastic process was used for all particles. The G4HadronElastic model was applied for all particles except for low energy neutrons for which the G4NeutronHPElastic model was preferred.

2.1.2. FLUKA. FLUKA (FLUKA-Website 2012) is a general purpose MC package for calculations of particle transport and interactions with matter, widely used for an extended range of applications including activation studies, dosimetry, and particle therapy (Ferrari *et al* 2005, Battistoni *et al* 2007, Battistoni *et al* 2008). In this work, the FLUKA 2012 development version, applying the default settings for hadron therapy ('*HADROTHE*'), was used. This version of FLUKA contains a few physics improvements with respect to the presently distributed public version. For the sake of this paper, the only differences are some refinements in prompt gamma generation (Böhlen *et al* 2013), whose impact is small for the distributions presented here, and a new treatment (Cerutti *et al* 2012, Böhlen *et al* 2013) of (p,d) and (n,d) reactions which improves significantly the agreement with experimental data for ^{12}C(p,x)^{11}C and ^{16}O(p,x)^{15}O excitation functions. These developments will be included in the

Table 1. Hadronic models used in the GATE/Geant4 simulations. The 'generic ions' correspond to ions heavier than alpha particles.

| Hadronic process	Particles	Geant4 processes	Geant4 models	Geant4 datasets	Energy range
Elastic scattering	All particles except low energy neutrons	G4HadronElastic Process	G4HadronElastic	G4HadronElastic DataSet	0–500 GeV
Elastic scattering	Low energy neutrons	G4HadronElastic Process	G4NeutronHPElastic	G4NeutronHPElastic Data	0–20 MeV
Inelastic process for protons	Protons	G4ProtonInelastic Process	G4BinaryCascade	G4ProtonInelastic Cross Section	0–500 GeV
Inelastic process for ions	GenericIon, Deuteron, Triton, ^{3}He, Alpha	G4IonInelastic Process	G4QMDReaction	G4IonsShen Cross Section	0–500 GeV
Inelastic scattering for neutrons	Neutron	G4NeutronInelastic Process	G4NeutronHPInelastic	G4NeutronHP InelasticData	0–20 MeV
			G4BinaryCascade	G4NeutronInelastic Cross Section	14 MeV–500 GeV
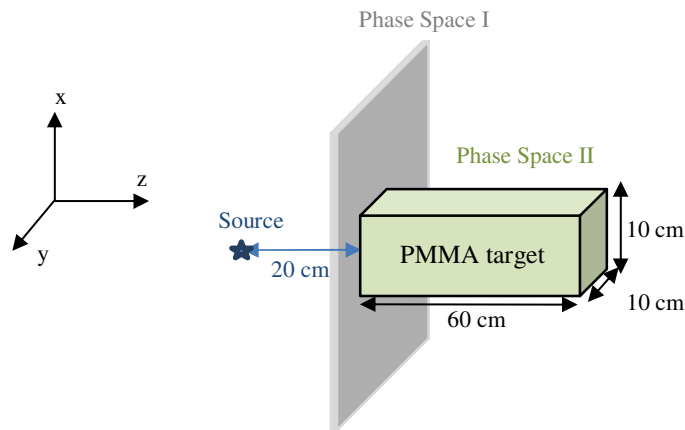
Figure 1. Set-up scheme.

new release of the code which will likely occur toward the end of 2013. In FLUKA, the choice of the pre-selected defaults (e.g. HADROTHE, PRECISIO, etc) does not impact the physics description which is unique and cannot be changed. The HADROTHE default was chosen here since it does not have uselessly low default transport thresholds, which would be very CPU demanding, but disposes, on the other hand, of a fine dE/dx mesh which facilitates accurate range predictions. Between 125 MeV and 5 GeV per nucleon, nucleus–nucleus interactions were treated with an extensively modified version (Andersen *et al* 2004) of the rQMD-2.4 (relativistic QMD) model (Sorge *et al* 1989), while the BME model was employed for an appropriate handling of interactions below an energy of 125 MeV per nucleon down to the Coulomb barrier (Cerutti *et al* 2006). Inelastic hadron–nucleus interactions were described by the PEANUT (pre-equilibrium-approach-to-nuclear-thermalization) model (Ferrari and Sala 1998, Ferrari and Sala 2002). Using hadron therapy default settings, the particle transport threshold for all hadrons was set to 1 keV, except for neutrons which were transported down to thermal energies.

2.2. Simulation set-ups

A simple geometry involving a homogeneous phantom was used to compare the two codes with a limited number of confounding factors.

For the proton therapy case, a perfect line beam (no angular spread) of 10^7 protons irradiating a $10 \times 10 \times 60$ cm^3 PMMA ($\rho = 1.19$ g cm^{-3}, $C_5H_8O_2$) target placed in air was simulated (figure 1). In all simulations, the ionization potential value of the PMMA was fixed to $I = 74$ eV. The monoenergetic protons (134 MeV) were produced by a point source located 20 cm upstream from the entrance of the target and hit the target at the center of the entrance side.

Exactly the same set-up (figure 1) was simulated for a monoenergetic 260 *A*MeV carbon beam using 10^6 primary ions.

2.3. Phase space files

To compare particle properties at different levels in the simulations, phase spaces, that contain the essential properties of the simulated particles at a given geometric level, were used. The features of interest of all particles entering the target were stored in a ROOT (ROOT-Website

2012) file (corresponding to phase space I, figure 1) in a dedicated TTree. This 'Incoming' TTree included ten variables: the event ID, the PDG (Particle Data Group, PDG-Website 2012) id number of the particle, the atomic and mass numbers of the particle, the (x, y, z) particle coordinates and the (p_x, p_y, p_z) particle momentum at the entrance of the target. Another TTree was used to store 15 features of interest of particles exiting from the target (phase space II—figure 1), namely all the variables included in the 'Incoming' TTree, the coordinates at which the particle was produced within the target as well as two temporal particle coordinates. The two temporal characteristics included the time of production of the secondary particle in the target (t_prod) and the time at which the secondary particle exited from the target (t_out).

2.4. Observables

2.4.1. Depth dose curves. The deposited dose was integrated in the *xy* plane. Depth dose curves computed along the main axis of the target, coinciding with the beam direction (*z* axis), were plotted with a 0.5 mm binning. Range estimations were conventionally calculated as the position of the 80% level of the distal fall-off.

2.4.2. Yields of particles exiting from the target. Using the PDG value, the number of particles exiting from the target (N_j) was integrated over the surface of the target for each particle type *j* (gammas, neutrons, protons, ions). Yields per primary were obtained by dividing N_j by the number of incident particles (protons or carbon ions).

2.4.3. Energy distributions of secondary particles. dN_j/dE energy distributions were plotted for outgoing prompt gammas (t_prod <10 ns) and protons using the particle momentum information. In the previous expression, dN_j is the number of particles of type *j* exiting from the target with an energy between E and $E + dE$. Depending on the considered secondary particles, either a 0.1 MeV (gammas) or a 1 MeV (proton) energy binning was used. For neutrons, 'lethargy' plots (equation (1)) were plotted to carefully analyze the low energy component. An energy-dependent binning (from 1.5 10^{-13} GeV at 1 10^{-13} GeV energy to 0.02 GeV at 0.13 GeV energy) was used.

$$\frac{dN_j}{d \, \text{Log} \, E} = E \frac{dN_j}{dE} \tag{1}$$

2.4.4. Angular and energy double-differential plots of the secondary particles. By analyzing the particle momentum at the exit of the target, double-differential plots in angle and energy were drawn for secondary gammas, neutrons and protons. The polar angle θ (figure 2, equation (2)) was calculated for each outgoing particle. In equation (2), px_{out}, py_{out} and pz_{out} correspond to the momentum components of the secondary particle at the exit of the target in the (O, x, y, z) referential.

$$\cos \theta = \frac{pz_{\text{out}}}{\left(px_{\text{out}}^2 + py_{\text{out}}^2 + pz_{\text{out}}^2\right)^{1/2}} \tag{2}$$

2.4.5. Production depth of secondary particles. The distributions of sites of $\beta+$ annihilations were calculated with the two MC codes. This allowed us to compare the performance of the hadronic models in the context of range monitoring using PET imaging. A time window ($\tau > 1$ ms), applied to the production time (t_prod), was used to differentiate annihilation photons from prompt gammas. A similar study was performed for prompt gamma emission.
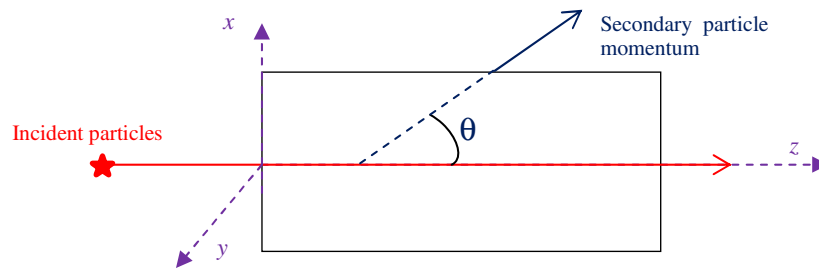
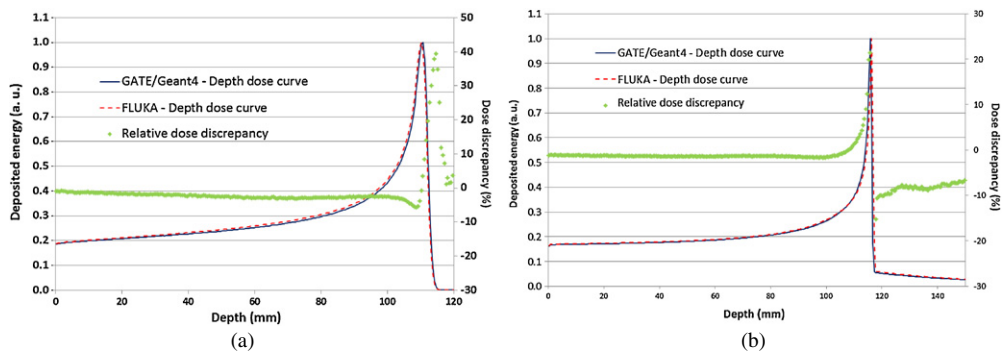**Figure 2.** Polar angle determination.

Figure 3. Depth dose curves in PMMA ($I = 74$ eV) obtained using GATE/Geant4 and FLUKA for monoenergetic (a) protons (134 MeV) and (b) carbon ions (260 AMeV). Point-to-point relative dose discrepancies between the two codes are superimposed.

In this case, only gammas that produced less than 10 ns after the end of the irradiation were selected. This 10 ns value was estimated by adding the transit time of incident particles from the source to the target to the order of magnitude of experimentally evaluated time-of-flight values (Le Foulher *et al* 2010). An energy threshold (E > 1 MeV) was additionally applied to keep only useful prompt gammas. Indeed, studies on prompt gamma detection for hadrontherapy monitoring have shown that an energy threshold of 1 MeV or more was necessary to get rid of most of the neutron-induced background (Min *et al* 2006, Testa *et al* 2009, Smeets *et al* 2012).

2.4.6. Time distribution of prompt gamma production.   The time distribution of prompt gamma production (*t_prod*) was plotted for the two codes. As for the production depth analysis, only gammas characterized by *t_prod* < 10 ns and E > 1 MeV were selected. Curves were normalized to the same area to compare the shapes more easily.

3. Results

3.1. Depth dose curves

Figure 3 shows the normalized depth dose curves in PMMA ($I = 74$ eV) obtained with GATE/Geant4 and FLUKA for the proton beam (134 MeV) (a) and for the carbon ion beam (260 AMeV) (b). Statistical errors were too small (<0.5% from 0 to 115 mm depths for protons and <0.3% from 0 to 170 mm depths for carbon ions) to be plotted in figure 3. The

Table 2. Yields of outgoing particles per primary particle obtained using GATE/Geant4 and FLUKA codes for a 134 MeV proton beam irradiating a homogeneous PMMA target.

	GATE/Geant4	FLUKA	Ratio
Gammas (>1 MeV)	0.094 496 ± 0.000 097	0.049 312 ± 0.000 070	1.92
Neutrons	0.087 136 ± 0.000 093	0.055 540 ± 0.000 074	1.57
Protons	0.001 292 ± 0.000 011	0.001 039 ± 0.000 010	1.24

Table 3. Yields of outgoing particles per primary particle obtained using GATE/Geant4 and FLUKA codes for a 260 AMeV carbon ion beam irradiating a homogeneous PMMA target.

	GATE/Geant4	FLUKA	Ratio
Gammas (>1 MeV)	0.916 02 ± 0.000 96	0.442 28 ± 0.000 66	2.07
Neutrons	2.9262 ± 0.0017	2.4884 ± 0.0016	1.17
Protons	0.401 70 ± 0.000 63	0.350 77 ± 0.000 59	1.14
Ions	0.059 52 ± 0.000 24	0.066 15 ± 0.000 26	0.89

point-to-point relative dose discrepancies between the two codes, i.e. the differences in normalized dose observed between the two codes at a certain depth, were superimposed. Using figure 3, range values of 111.69 and 116.09 mm for GATE and 111.40 and 116.55 mm for FLUKA were obtained for protons and carbon ions respectively.

3.2. Yields of secondary particles exiting the target

Tables 2 and 3 show the yields of secondary particles exiting from the target obtained with the two codes for the proton and carbon ion beams. For photons, only gammas useful for dose monitoring based on prompt gamma imaging (E > 1 MeV) were analyzed.

3.3. Energy distribution of secondary particles

Energy distributions corresponding to all outgoing gammas (neither energy nor time selection) are shown in figure 4. As observed in section 3.2, GATE/Geant4 over-estimates production yields of gammas as obtained with FLUKA regardless of the energy. Differences in photon yields between GATE/Geant4 and FLUKA as large as 6.7 and 7.4 were obtained at some energies, for proton and carbon ion beams, respectively. For annihilation photons ($t\_prod >$ 1 ms), the ratio between the number of gammas produced by GATE to the number of gammas produced by FLUKA is equal to 1.09 and 1.20 for the proton beam and the carbon ion beam, respectively.

The energy distributions of outgoing protons obtained with GATE/Geant4 and FLUKA are shown in figure 5 for the proton beam and the carbon ion beam. Despite the fact that the shapes of the distributions are similar for the two codes, slight discrepancies in magnitude are observed for proton (figure 5(a)) as well as for carbon ion beams (figure 5(b)). For both incident beams, GATE/Geant4 predicts a somewhat higher number of secondary protons over most of the energy range.

Figure 6 shows lethargy plots corresponding to outgoing neutrons obtained with GATE/Geant4 and FLUKA for the proton and the carbon ion beams. For both beams, GATE/Geant4 overestimated the leakage of neutrons with energies from 1 eV to 100 MeV
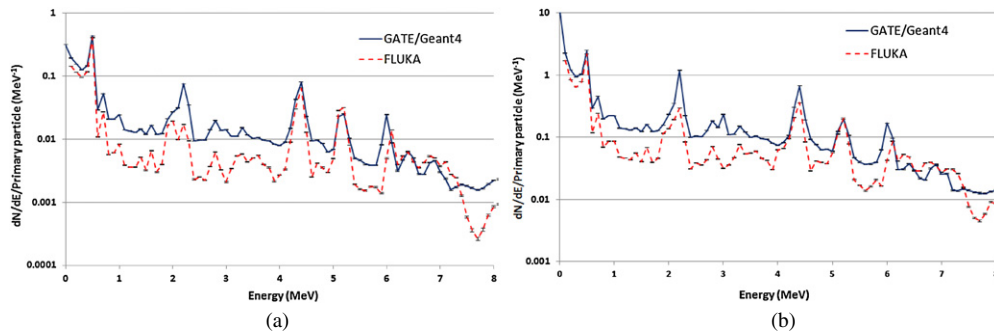
Figure 4. Outgoing gamma energy distributions per primary particle obtained with GATE/Geant4 and FLUKA for monoenergetic (a) protons (134 MeV) and (b) carbon ions (260 *A*MeV) irradiating a PMMA target. Neither energy nor time selection were used.
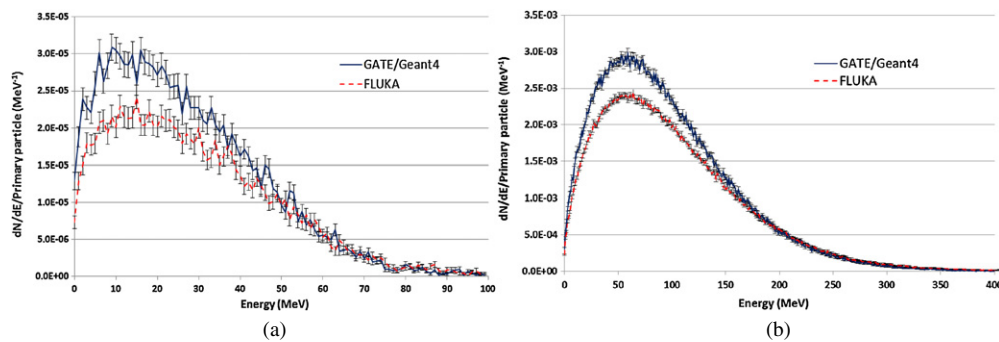

Figure 5. Outgoing proton energy distributions per primary particle obtained with GATE/Geant4 and FLUKA for monoenergetic (a) protons (134 MeV) and (b) carbon ions (260 *A*MeV) irradiating a PMMA target.
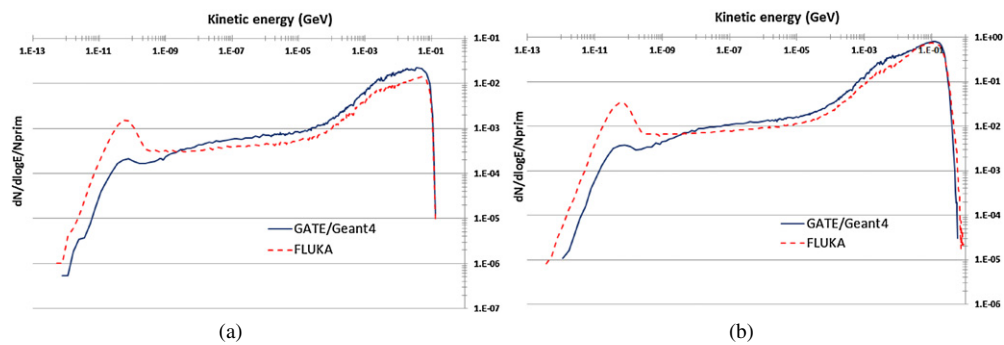

Figure 6. Lethargy plots corresponding to outgoing neutrons obtained using GATE/Geant4 and FLUKA for monoenergetic (a) protons (134 MeV) and (b) carbon ions (260 *A*MeV) irradiating a PMMA target.

compared to FLUKA. An average overestimation of 1.5 was calculated for this energy range. Large discrepancies were also observed for energies lower than 1 eV: for these energies,
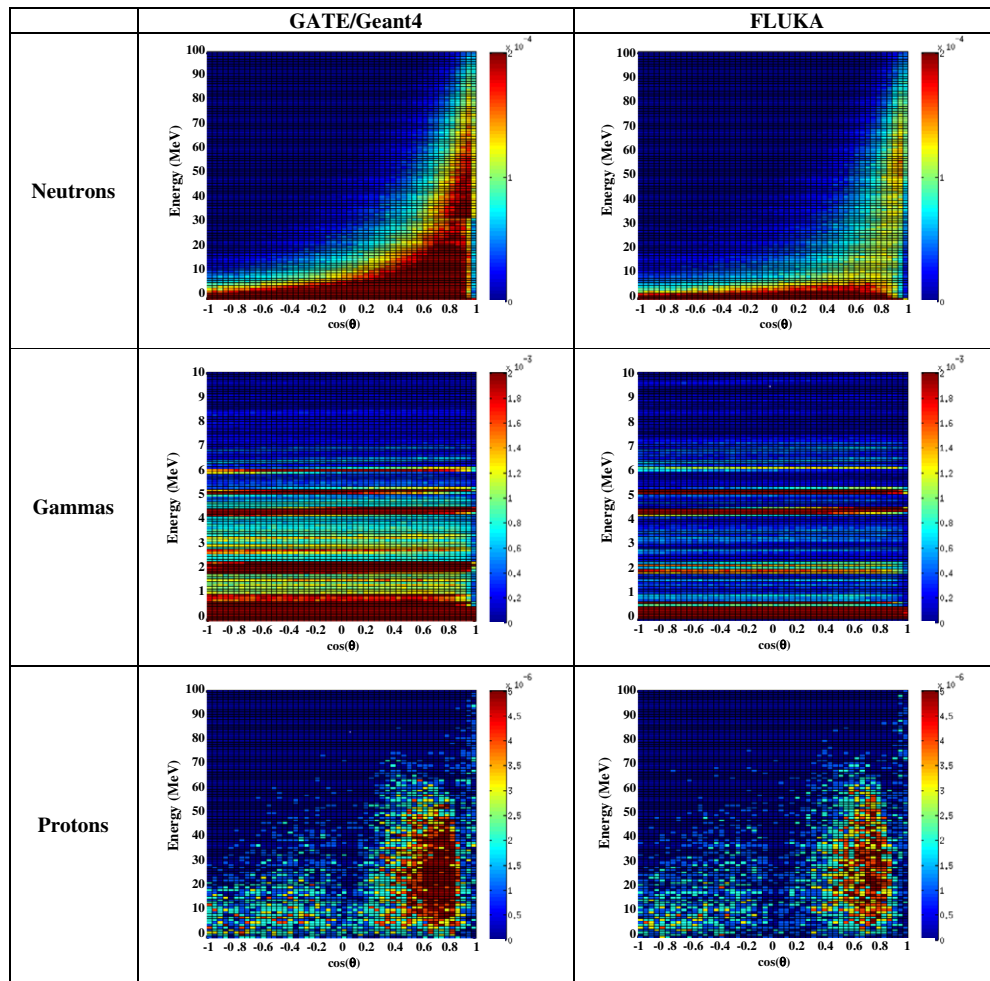
Figure 7. Angular and energy double-differential plots of outgoing neutrons, gammas and protons ($MeV^{-1}\,sr^{-1}$) produced by the irradiation of a PMMA target by monoenergetic (134 MeV) protons, as predicted by GATE/Geant4 and FLUKA. For gammas, neither energy nor time selection were used.

FLUKA predicted about 3.5 times larger neutron leakage than GATE/Geant4. For carbon ions, a good agreement was observed from 30 to 300 MeV with maximum relative differences of 15% (figure 6(b)).

3.4. Angular and energy double-differential plots of secondary particles

Figures 7 and 8 show the angular and energy double-differential plots obtained with GATE/Geant4 and FLUKA for the proton beam and the carbon ion beam. Plots corresponding to three types of particles (neutrons, gammas and protons) are displayed. For gammas, neither energy nor time selection were used.
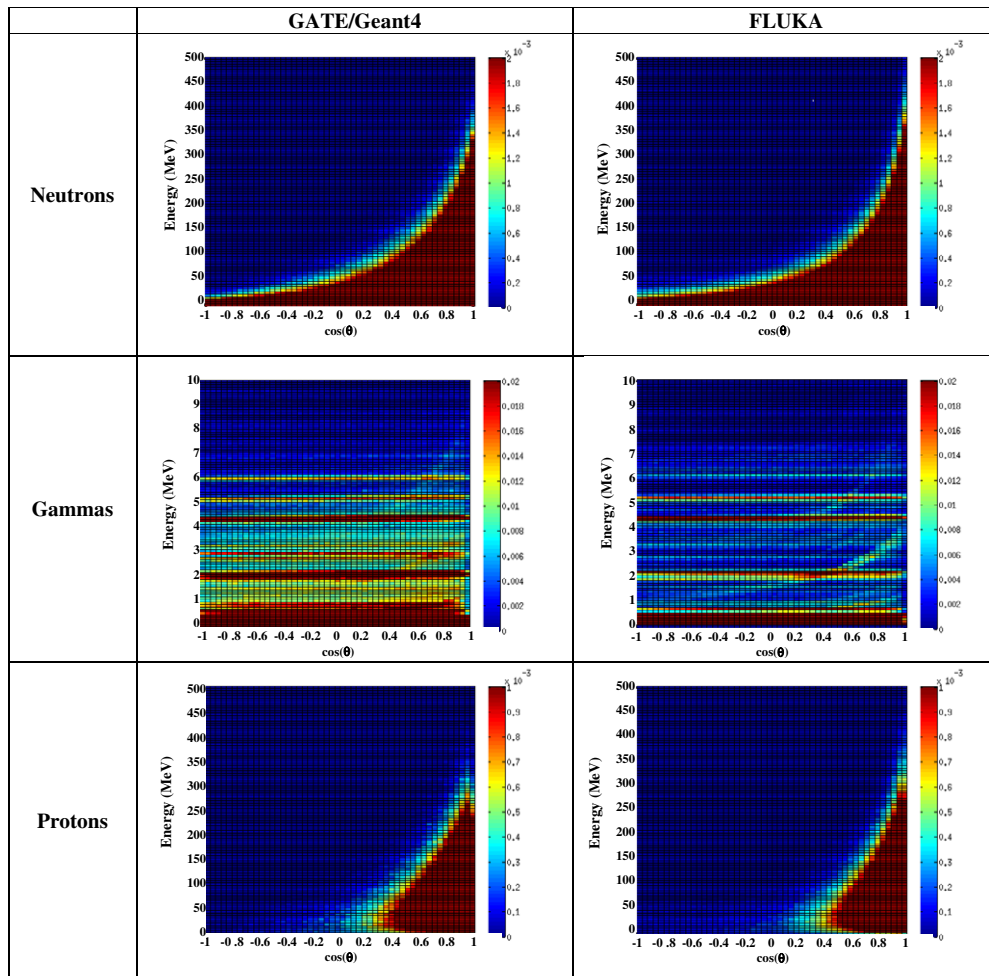
	GATE/Geant4	FLUKA
Neutrons		
Gammas		
Protons		

Figure 8. Angular and energy double-differential plots of outgoing neutrons, gammas and protons (MeV^{-1} sr^{-1}) produced by the irradiation of a PMMA target by monoenergetic (260 *A*MeV) carbon ions, as predicted by GATE/Geant4 and FLUKA. For gammas, neither energy nor time selection were used.

3.5. Production depth of secondary particles

Figure 9 compares the location of production of the outgoing annihilation photons (*t_prod* > 1 ms, no energy discrimination) along depth generated by the GATE/Geant4 and FLUKA simulations. For the proton beam (figure 9(a)), the most important difference concerns the distal fall-off region. The slope of this region, that is steeper in the GATE/Geant4 simulations, leads to a significant discrepancy in the determination of the fall-off position (defined as the depth at 80% of the maximum): 105.20 mm for GATE against 103.54 mm in the FLUKA simulations. This 1.66 mm difference is quite significant compared with the 0.29 mm difference observed in the proton ranges (figure 3(a)). For the carbon ion beam, global shapes are fairly similar between the two codes except at the end of the range of the carbon ions (figure 9(b)). Differences in the amplitudes of the production peaks (ratio of 1.22) as well as in the fragmentation tails are observed. 114.87 mm and 116.70 mm fall-off positions
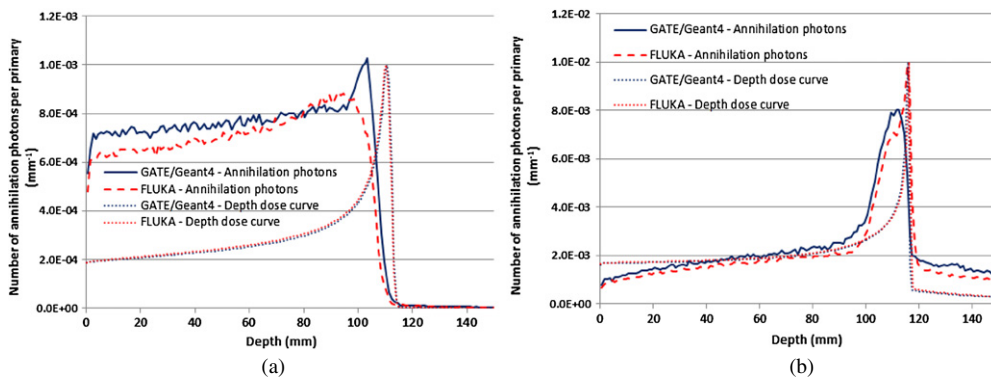
Figure 9. Comparison of the location of production of the annihilation photons (*t_prod* > 1 ms, no energy discrimination) exiting from the target obtained using GATE/Geant4 and FLUKA for (a) the proton beam (134 MeV) (b) the carbon ion (260 *A*MeV) beam.
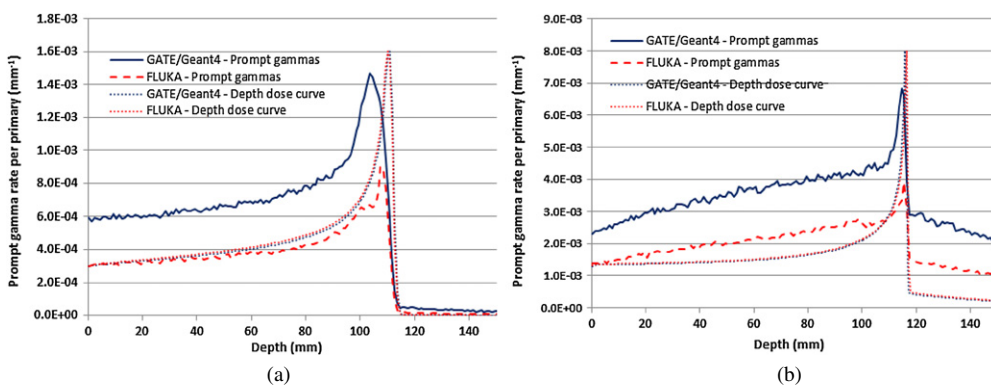

Figure 10. Comparison of the location of production of the prompt gammas exiting from the target obtained using GATE/Geant4 and FLUKA for (a) the proton beam (134 MeV) (b) the carbon ion (260 *A*MeV) beam.

were determined from figure 9(b). This 1.83 mm difference between the two codes is higher than the 0.46 mm difference already observed comparing the carbon ion ranges (figure 3(b)).

Figure 10 compares the location of production of the outgoing prompt gammas (*t_prod* < 10 ns, E > 1 MeV).

For protons (figure 10(a)), in addition to the production yield discrepancy, a difference is observed in the determination of the fall-off position (defined as the depth at 80% of the maximum): 108.40 mm for GATE/Geant4 against 109.68 mm in the FLUKA simulations. This 1.2% difference is mainly due to the shape of the distal fall-off that is sharper in the FLUKA simulations. For carbon ions (figure 10(b)), values of 115.94 mm and 116.49 mm are obtained for GATE/Geant4 and FLUKA respectively. This 0.55 mm difference (0.5%) between the two codes is negligible given the 0.46 mm difference already observed when comparing the carbon ion ranges (figure 3(b)).

3.6. Prompt gamma time distribution

Comparisons of the times of production of the prompt gammas predicted by the two codes are shown in figure 11 for the proton beam and for the carbon ion beam, where curves were
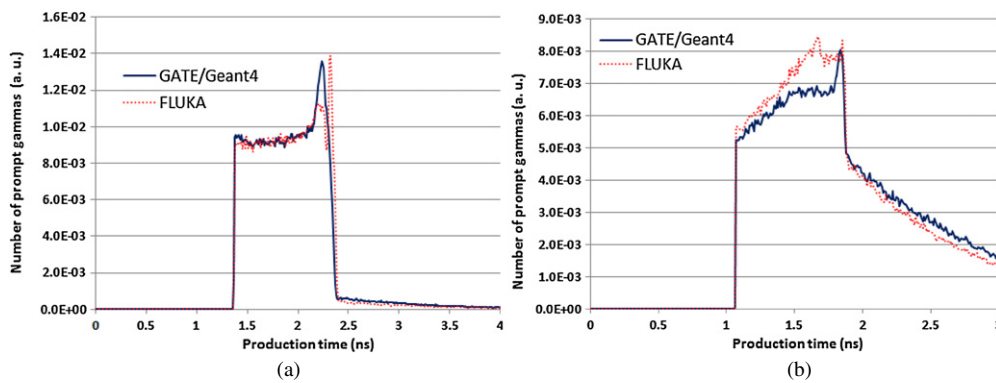
Figure 11. Time distributions of prompt gamma productions obtained using GATE/Geant4 and FLUKA for (a) the proton (134 MeV) beam, (b) the carbon ion (260 *A*MeV) beam.

normalized to the same area. The $t = 0$ value corresponds to the time at which incident particles (protons or carbon ions) are produced. For the proton beam (figure 11(a)), a good agreement in shape is observed between the two codes except for the last part ($2.1 < t\_prod < 2.4$ ns). On the contrary, discrepancies are observed for $t\_prod < 1.8$ ns for the carbon ion beam (figure 11(b)).

4. Discussion

As already demonstrated by recent studies (Seravalli *et al* 2012), a good agreement between GATE/Geant4 and FLUKA was obtained for depth dose deposit. The differences in range were respectively equal to 0.29 mm (0.3% of the range) and 0.46 mm (0.4% of the range) for protons (134 MeV) and carbon ions (260 *A*MeV) irradiating a PMMA target (figure 3). These differences, lower than 1% of the range, fulfill the dose precision requirement. Point-to-point relative dose discrepancies between the two codes (figure 3) confirm this good agreement: mean discrepancies of 2.3% and 0.8% were observed in front of the Bragg peak for protons and carbon ions respectively. These results, combined with the comparison of each code to experimental data (Parodi *et al* 2007b, Koch *et al* 2008, Grévillot *et al* 2010), validates the modeling of the dose deposit in the beam direction for the two codes.

Despite the very simple target and set-up, discrepancies were observed between the codes when comparing the spatial and time distributions of secondary particles exiting the PMMA target. In the next paragraphs, results are analyzed for each observable and each particle type. Comparisons to experimental data are also discussed to facilitate the interpretation of the simulated results.

Regarding outgoing high energy (>1 MeV) gamma yields, ratios of 1.92 and 2.07 were obtained between GATE/Geant4 and FLUKA for proton and carbon ion beams, respectively (tables 2 and 3). Comparing Geant4 9.1 simulations to experimental data, (Le Foulher *et al* 2010) showed that Geant4 simulations overestimated prompt-gamma ray detection yields by a factor of 12. These results, obtained with an old version of Geant4, included only the prompt gammas emitted with a 90° angle with respect to the beam direction and depositing energies higher than 2 MeV. Though they cannot be compared directly to our results, they show that an improvement of Geant4 hadronic models is needed. For that purpose, work on the dynamic part describing ion–ion collisions and mainly the QMD model is in
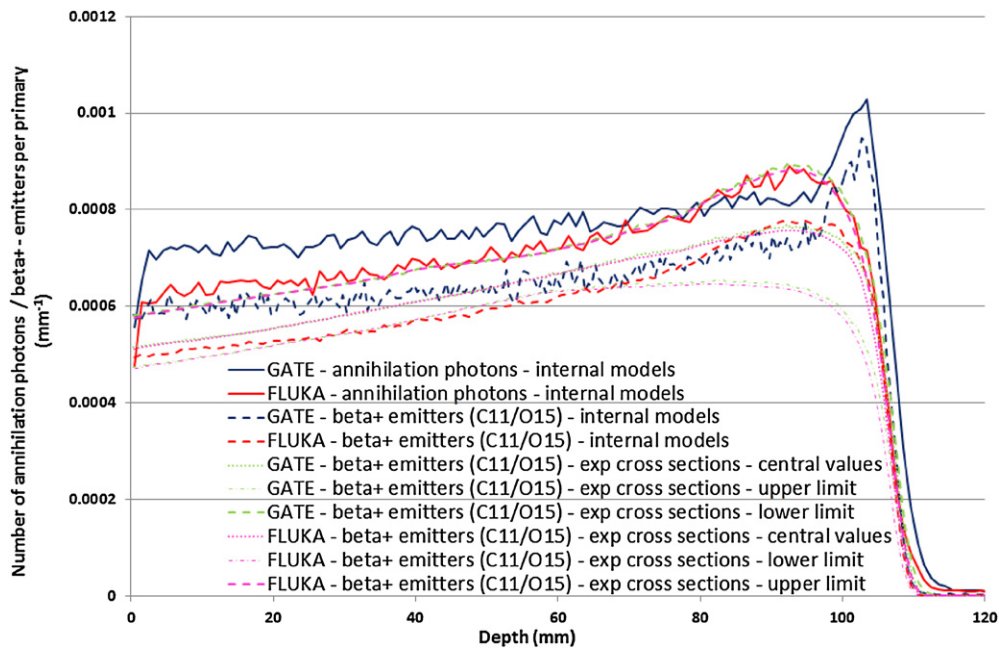
Figure 12. Depths of production of the $\beta+$ emitters (^{11}C, ^{15}O) obtained combining the fluence of the protons in the PMMA target (GATE/Geant4 and FLUKA) to experimental cross-sections compared to the depths of production of the annihilation photons and depths of production of the $\beta+$ emitters (^{11}C, ^{15}O) obtained using the internal models of GATE/Geant4 and FLUKA.

progress. The de-excitation stage (statistical part) was also recently improved by the Geant4 developers by including the Fermi break-up as a default option (Geant4-Website 2012c). These improvements lead to an overestimation of the detected prompt-gamma yield by a factor of 2 today (ENVISION deliverable 2012). The experimental prompt gamma yield can however be accurately reproduced with Geant4 by tuning the tolerance factor of the photon evaporation model (Lestand *et al* 2012). FLUKA reproduced the above measurements (Le Foulher *et al* 2010) within 10–15% (Böhlen *et al* 2013). A more detailed comparison of FLUKA with experimental prompt gamma yields will be presented separately in an upcoming paper.

In figure 4, the comparison of outgoing gamma energy distributions shows that the prompt gamma yield predicted by GATE/Geant4 exceeds that predicted by FLUKA for the entire energy spectrum (0–8 MeV), except for the energy region where the contribution from annihilation photons dominates. The agreement between the two codes observed in the 501–521 keV range (differences within 6% for *t_prod* > 1 ms) is important when using simulations for assisting the development of $\beta+$ imaging systems. Indeed, prototyping such new systems often requires an accurate estimate of the gamma annihilation yields in order to adjust the efficiency of the system.

Figure 9 compares the positions of production of the annihilation photons. It confirms the fairly good agreement between the two codes. It however also shows some discrepancies higher than 1 millimeter in the range determination. These differences in the distal fall-off might have a significant impact on the determination of the range of the incident particles based on PET imaging. Previous works (Parodi *et al* 2002, 2005, Espana *et al* 2011, Seravalli *et al* 2012) resorted to a convolution of simulated particle fluences with experimental cross-section data in order to overcome possible deficiencies in the code internal models. Figure 12 depicts the depth

of production of the $\beta+$ emitters (^{11}C, ^{15}O) due to the reactions (^{12}C(p,x)^{11}C, ^{16}O(p,x)^{15}O) obtained by combining the fluence of the protons in the PMMA target (GATE/Geant4 and FLUKA simulations) with experimental cross-sections (Parodi *et al* 2002, EXFOR-Website 2012), compared to the positions of production of the annihilation photons (figure 9(a)) and $\beta+$ emitters (^{11}C, ^{15}O) obtained using GATE/Geant4 and FLUKA internal models. As in all the study, 134 MeV monoenergetic protons were considered. A multiplication by a factor of 2 was applied to the $\beta+$ emitter curve in order to mimic the production of two annihilation photons per $\beta+$ disintegration. The lower and upper boundary curves for the experimental cross-sections were derived from the EXFOR database (EXFOR-Website 2012), while the central fit has been taken from (Parodi *et al* 2002). The simulated depths of production of the $\beta+$ emitters obtained using the proton fluences computed with GATE/Geant4 or FLUKA folded with the central fit were already validated against experimental data (Parodi *et al* 2002, Seravalli *et al* 2012). The difference between the FLUKA and GATE/Geant4 internal models was quite important. Results simulated with FLUKA internal models better reproduced the shape and magnitude of the curves based on experimental cross-sections. The Geant4 BiC model has therefore to be improved in order to suppress the ^{11}C production peak at the end of the proton range. It is also well visible that the convolution method, if limited to these two reactions, underestimates the total production of $\beta+$ emitters, since it does not account for all the possible reaction channels leading to $\beta+$ emitter production. The comparison of the experimental back-projected activity distributions of annihilation photons produced by carbon ion beams in PMMA with simulated results obtained with an older version of FLUKA can be found in Sommerer (2007) and Sommerer *et al* (2009). In the results presented here, an improved version of the BME model (Cerutti *et al* 2012) has been used.

GATE/Geant4 strongly overestimated the outgoing neutron production yield predicted by FLUKA in proton therapy ($+57\%$) (table 2). A lower difference was observed for carbon ions with a 17% greater yield with GATE/Geant4 compared to FLUKA (table 3). Experimental data exist about neutron production generated by proton or carbon ion beams on both thin and thick targets (Kurosawa *et al* 1999, Gunzert-Marx *et al* 2008, Braunn *et al* 2009, Bedogni *et al* 2012, Iwamoto *et al* 2012). Gunzert-Marx *et al* (2008) give experimental values considering a 200 *A*MeV carbon ion beam irradiating a 12.78 cm thick water target. In this study, a 0.54 ± 0.11 neutron production yield was obtained in the forward hemisphere. Only neutrons with an energy >20 MeV were considered. The same set-up as the one described in Gunzert-Marx *et al* (2008) was simulated in GATE/Geant4 and we observed a 0.79 production yield. Results, which overestimated the experimental data by about 46%, are, however, in the same order of magnitude given the large uncertainty affecting the experimental data. Indeed, only four angular distributions from $0°$ to $30°$ were measured. The 0.54 fragment yield was obtained by integration of extrapolating exponential functions.

Regarding outgoing neutron energy distributions (figure 6), discrepancies were observed between GATE/Geant4 and FLUKA for proton and carbon ion beams for the entire energy range and more particularly for thermal neutrons with energies lower than 0.5 eV. For these energies, FLUKA predicted about 3.5 times larger neutron leakage than GATE/Geant4. Neutrons produced from nuclear reactions are of much higher energy, hundreds of keV and above. They are subsequently moderated, mostly because of the hydrogen content, down to thermal energies. Given the much smaller discrepancies between the two codes at energies above 100 keV, only a difference between the two codes in neutron transport and moderation might explain this finding. FLUKA has been extensively benchmarked in similar conditions. For example, it has been shown to reproduce accurately the moderation down to thermal energies and eventual detection of neutrons in polyethylene spheres irradiated with calibrated monoenergetic neutron beams (Birattari *et al* 1998). Figure 13 shows the neutron energy
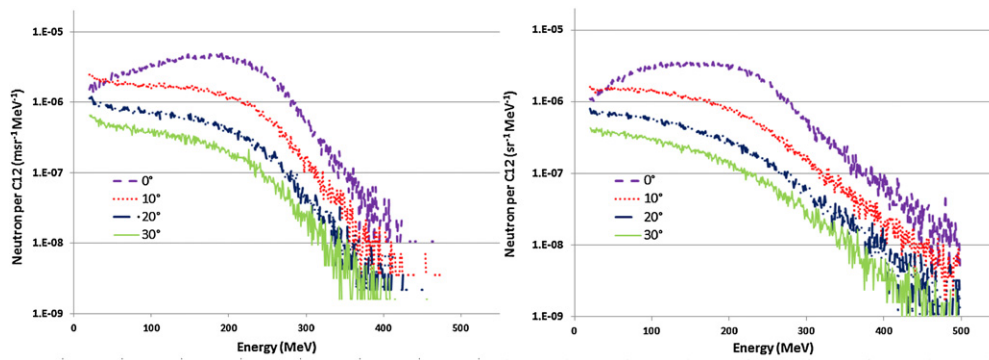
Figure 13. Energy spectra of outgoing neutrons corresponding to 0°, 10°, 20° and 30° angles obtained using GATE/Geant4 (left) and FLUKA (right) for the carbon ion beam (260 *A*MeV) configuration.

spectra obtained using GATE/Geant4 and FLUKA at 0°, 10°, 20° and 30° angles for the carbon ion beam for neutron energies >20 MeV. At small angles, a broad maximum was observed at about half of the projectile energy per nucleon (130 MeV) for the FLUKA code. This maximum was moved forward higher energies (∼200 MeV) in GATE simulations. At larger angles, no maximum was observed and the neutron emission yield decreased when energies increased. Finally, the maximum neutron energy was about twice the incident particle energy per nucleon in FLUKA simulations but smaller in GATE simulations (∼420 MeV). These observations suggest that FLUKA simulations better reproduce observations related to neutron production compared to GATE/Geant4 (Gunzert-Marx *et al* 2008).

In this study, only secondary neutrons produced inside the PMMA target were considered. In a clinical setting, the treatment nozzle highly contributes to the amount of secondary neutrons, especially in passive scattered proton therapy (Zheng *et al* 2007). It should thus be simulated for experimental validation of the neutron energy spectra. GATE and FLUKA MC codes were used to evaluate the secondary neutron dose resulting from two different collimators in protontherapy (Moskvin *et al* 2012, Diffenderfer *et al* 2012). These two studies, that led to opposite conclusions for the two codes, clearly highlighted the need for comparison studies between MC codes.

Protons exiting from the target are increasingly studied in carbon ion therapy (Henriquet *et al* 2012). Carbon ions lead indeed to high proton production yields, comparable to the yields of prompt gamma of energies >1 MeV (table 3), and can be detected with intrinsic efficiencies close to 1. They can therefore be a good alternative to annihilation photons and prompt gammas for ion range monitoring in hadrontherapy. In this study, a fairly good agreement was obtained between the two codes regarding the proton yield in carbon ion therapy (ratio equal to 1.14—table 3). As for the outgoing neutron comparison, the experimental set-up proposed by (Gunzert-Marx *et al* 2008) was simulated in GATE/Geant4. A 0.32 production yield was obtained. This yield overestimated the 0.20 ± 0.03 experimental value obtained in Gunzert-Marx *et al* (2008). Figure 14 compares the energy spectra of secondary protons obtained with GATE/Geant4 and FLUKA at 0°, 10°, 20° and 30° angles for the carbon ion beam for proton energies larger than 20 MeV. As observed in the experimental study, the shapes of the proton and neutron energy spectra were similar for 10°, 20° and 30° angles. However, contrary to the neutron spectra, the maxima were not observed at about 130 MeV for the 0° angle neither with
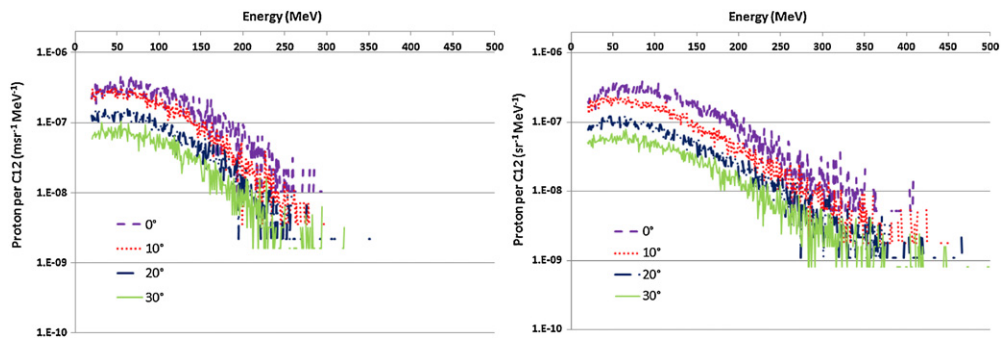
Figure 14. Energy spectra of secondary protons corresponding to 0°, 10°, 20° and 30° angles obtained using GATE (left) and FLUKA (right) for the carbon ion beam (260 *A*MeV) configuration.

GATE/Geant4 nor with FLUKA. With FLUKA, the proton spectra extended to about twice the energy per nucleon of the primary ions which is in good agreement with experimental data.

Figures 7 and 8 summarize the angular and energy distributions of all particles of interest for the *in-vivo* treatment verification in hadrontherapy. An overall good agreement in shapes was obtained between the two codes for the two treatment modalities except for forward high energy neutrons in the proton beam configuration. These graphs are of foremost importance for optimizing the positioning of proton imaging systems in carbon ion therapy.

In protontherapy and carbon ion therapy, conventional beams have energies ranging from 70 to 250 MeV and from 50 to 430 *A*MeV. In this study, only results corresponding to intermediate energies were presented. The same comparison was also carried out for lower energies of 70 MeV (proton beam) and 130 *A*MeV (carbon ion beam). Results showed that trends observed at intermediate energies could be extended to lower energies for prompt gammas and annihilation photons. For secondary neutrons and protons, conclusions about the comparison of the two codes can be slightly different as a function of the beam energy. For example, a better agreement between the two codes was observed in the production yield (0.98 ratio between GATE/Geant4 and FLUKA for a 70 MeV energy against 1.24 for the 134 MeV beam) as well as in the energy spectra of secondary protons at low energy for the proton beam. On the contrary, discrepancies between GATE/Geant4 and FLUKA increased when comparing neutron production yields predicted by the two codes for the carbon ion beam (1.68 ratio against 1.17 for the 260 *A*MeV beam).

Different physics lists have been tested during this work for GATE/Geant4 simulations. The physics list proposed in section 2.1.1 provided the best agreement compared to experimental data in the context of dose monitoring based on emission tomography systems in hadrontherapy. Compared to the set of parameters described in Jarlskog and Paganetti (2008), a different inelastic process was used for ions, and the G4HadronElastic process was used instead of the G4UHadronElastic recommended by Jarlskog and Paganetti (2008) for elastic interactions. The use of the G4UHadronElastic process can attenuate the discontinuity observed at 32 MeV in the angular and energy double-differential plot of outgoing neutrons (figure 7) (Jarlskog and Paganetti 2008). It is, however, no longer available in the last version of Geant4 (9.5). For FLUKA, no change of the physics models is possible and the default ones were therefore used for this comparison. The settings described in this paper are strongly recommended to people using GATE/Geant4 or FLUKA, limited to the production/transport cuts in this case, for the prototyping of secondary particle imaging systems. The results reported

in this study could also be used for checking that the codes are properly used, for the validation of new versions of the codes and/or for analysis of the results provided by other codes.

5. Conclusion

Energy and angular distributions of secondary emissions of foremost importance for the *in-vivo* treatment verification in hadrontherapy have been compared for two simulation tools, FLUKA and GATE/Geant4. Set-ups involving monoenergetic protons (134 MeV) and carbon ions (260 *A*MeV) irradiating a homogeneous PMMA target have been studied.

For proton and carbon ion beams, the codes predict yields of annihilation photons differing by less than 20% while the yields of useful prompt-gamma rays differ significantly (∼100% for proton and carbon ion beams). This first result is promising for the prototyping of new PET imaging systems using MC codes. For neutrons and protons, discrepancies in the production yields have been highlighted especially for the proton beam configuration. For outgoing neutrons, differences in shape in the energy spectra were also observed. The comparison to experimental data seems to argue in favor of the FLUKA results. Additional experimental data are still needed to further evaluate the quality of the nuclear fragmentation models implemented in Geant4 and FLUKA for the production of secondary emissions. A similar study involving a heterogeneous phantom including muscle and lung tissues is currently being carried out, to compare the two MC codes in a more realistic case.

Acknowledgments

References

Agostinelli S, Allison J, Amako K, Apostolakis J and Araujo H 2003 Geant4—a simulation toolkit *Nucl. Instrum. Methods* A **506** 250–303

Andersen V *et al* 2004 The FLUKA code for space applications: recent developments *Adv. Space Res.* **34** 1302–10

Battistoni G *et al* 2007 The FLUKA code: description and benchmarking *AIP Conf. Proc.* **896** 31–49

Battistoni G *et al* 2008 The FLUKA code and its use in hadron therapy ll *Nuovo Cimento* C **31** 69–75

Bedogni R, Amgarou K, Domingo C, Russo S, Cirrone G A P, Pelliccioni M, Esposito A, Pola A, Introini M V and Gentile A 2012 Measurement of neutron spectra generated by a 62 AMeV carbon ion beam on a PMMA phantom using extended range Bonner sphere spectrometers *Nucl. Instrum. Methods* A **681** 110–5

Birattari C, Esposito A, Ferrari A, Pelliccioni M, Rancati T and Silari M 1998 The extended range neutron rem counter 'LINUS': overview and latest developments *Radiat. Prot. Dosim.* **76** 135–48

Böhlen T T, Cerutti F, Dosanjh M, Ferrari A, Gudowska I, Mairani A and Quesada J M 2010 Benchmarking nuclear models of FLUKA and Geant4 for carbon ion therapy *Phys. Med. Biol.* **55** 5833–47

Böhlen T T *et al* 2013 The FLUKA code: developments and challenges for high energy and medical applications *Int. Conf. on Nuclear Data for Science and Technology (New York, 4–8 March)* at press

Bom V, Joulaeizadeh L and Beekman F 2012 Real-time prompt gamma monitoring in spot-scanning proton therapy using imaging through a knife-edge-shaped slit *Phys. Med. Biol.* **57** 297–308

Braunn B *et al* 2009 12C nuclear reaction measurements for hadrontherapy *12th Int. Conf. on Nuclear Reaction Mechanisms (Varenna, Italy)* pp 531–7

Cerutti F, Ferrari A, Mairani A and Sala P R 2012 New developments in FLUKA *13th Int. Conf. on Nuclear Reaction Mechanisms (Varenna, Italy)* pp 469–75

Cerutti F *et al* 2006 Low energy nucleus-nucleus reactions: the BME approach and its interface with FLUKA *11th Int. Conf. on Nuclear Reaction Mechanisms (Varenna, Italy)* vol 126 pp 507–11

Diffenderfer E S, Ainsley C G, Kirk M L, McDonough J E and Maughan R L 2012 Reply to 'comment on 'comparison of secondary neutron dose in proton therapy resulting from the use of a tungsten alloy MLC or a brass collimator system" *Med. Phys.* **39** 2306–9

ENVISION deliverable 2012 D3.1 compilation of gamma ray yield data http://cern.ch/ENVISION

Espana S, Zhu X, Daartz J, El Fakhri H, Bortfeld T and Paganetti H 2011 The reliability of proton-nuclear interaction cross-section data to predict proton-induced PET images in proton therapy *Phys. Med. Biol.* **56** 2687–98

EXFOR-Website 2012 www-nds.iaea.org/exfor/exfor.htm

Ferrari A and Sala P R 1998 The physics of high energy reactions *Workshop on Nuclear Reaction Data and Nuclear Reactors Physics, Design and Safety* vol 2 pp 424–532

Ferrari A and Sala P R 2002 Nuclear reactions in Monte Carlo codes *Radiat. Prot. Dosim.* **99** 29–38

Ferrari A, Sala P R, Fassö A and Ranft J 2005 FLUKA: a multi-particle transport code CERN Yellow Report 2005-10 No. CERN 2005-10, INFN/TC 05/11, SLAC-R-773

FLUKA-Website 2012 www.fluka.org

Frandes M, Zoglauer A, Maxim V and Prost R 2010 A tracking Compton-scattering imaging system for hadron therapy monitoring *IEEE Trans. Nucl. Sci.* **57** 144–50

GATE-Website 2012 www.opengatecollaboration.org

Geant4-Website 2012a http://geant4.cern.ch/results/validation_plots.htm

Geant4-Website 2012b http://geant4.cern.ch/

Geant4-Website 2012c http://geant4.cern.ch/support/ReleaseNotes4.9.5.html

Grevillot L, Bertrand D, Dessy F, Freud N and Sarrut D 2012 GATE as a GEANT4-based Monte Carlo platform for the evaluation of proton pencil beam scanning treatment plans *Phys. Med. Biol.* **57** 4223–44

Grevillot L, Frisson T, Zahra N, Bertrand D, Stichelbaut F, Freud N and Sarrut D 2010 Optimization of GEANT4 settings for proton pencil beam scanning simulations using GATE *Nucl. Instrum. Methods* B **268** 3295–305

Gunzert-Marx K, Iwase H, Schardt D and Simon R S 2008 Secondary beam fragments produced by 200 MeV/u ^{12}C ions in water and their dose contributions in carbon ion therapy *New J. Phys.* **10** 075003

Gunzert-Marx K, Schardt D and Simon R S 2004 Fast neutrons produced by nuclear fragmentation in treatment irradiations with ^{12}C beam *Radiat. Prot. Dosim.* **110** 595–600

Haettner E, Iwase H and Schardt D 2006 Experimental fragmentation studies with ^{12}C therapy beams *Radiat. Prot. Dosim.* **122** 485–7

Henriquet P *et al* 2012 Interaction vertex imaging (IVI) for carbon ion therapy monitoring: a feasibility study *Phys. Med. Biol.* **57** 4655–69

Iwamoto Y, Hagiwara M, Matsumoto T, Masuda A, Iwase H, Yashima H, Shima T, Tamii A and Nakamura T 2012 Measurements and Monte-Carlo calculations of forward angle secondary neutron production cross-sections for 137 and 200 MeV proton-induced reactions in carbon *Nucl. Instrum. Methods* A **690** 10–16

Jan S *et al* 2011 GATE V6: a major enhancement of the GATE simulation platform enabling modeling of CT and radiotherapy *Phys. Med. Biol.* **56** 881–901

Jarlskog C Z and Paganetti H 2008 Physics settings for using the Geant4 toolkit in proton therapy *IEEE Trans. Nucl. Sci.* **55** 1018–25

Kim C H, Park J H, Seo H and Lee H R 2012 Gamma electron vertex imaging and application to beam range verification in proton therapy *Med. Phys.* **39** 1001–5

Knopf A, Parodi K, Paganetti H, Cascio E, Bonab A and Bortfeld T 2008 Quantitative assessment of the physical potential of proton beam range verification with PET/CT *Phys. Med. Biol.* **53** 4137–51

Koch N, Newhauser W D, Titt U, Gombos D, Coombes K and Starkschall G 2008 Monte Carlo calculations and measurements of absorbed dose per monitor unit for the treatment of uveal melanoma with proton therapy *Phys. Med. Biol.* **53** 1581–94

Kurosawa T, Nakaruma T, Nakao N, Shibata T, Uwamino Y, Nakanishi N, Fukumura A and Murakami K 1999 Measurements of secondary neutrons produced from thick targets bombarded by high-energy helium and carbon ions *Nucl. Sci. Eng.* C **132** 30–56

LANL 2008 MCNPX 2.6.0 Users's Guide 2008

Lechner A, Ivanchenko V N and Knobloch J 2010 Validation of recent Geant4 physics models for application in carbon ion therapy *Nucl. Instrum. Methods* B **268** 2343–54

Le Foulher F *et al* 2010 Monte Carlo simulations of prompt gamma emission during carbon ion irradiation *IEEE Trans. Nucl. Sci.* **57** 2768–72

Lestand L, Montarou G, Force P and Pauna N 2012 In-beam quality assurance using induced $\beta+$ activity in hadrontherapy: a preliminary physical requirement study using Geant4 *Phys. Med. Biol.* **57** 6497–518

Mairani A, Brons S, Cerutti F, Fasso A, Ferrari A, Krämer M, Parodi K, Scholz M and Sommerer F 2010 The FLUKA Monte Carlo code coupled with the local effect model for biological calculations in carbon ion therapy *Phys. Med. Biol.* **55** 4273–89

Min C H, Kim C H, Youn M Y and Kim J W 2006 Prompt gamma measurements for locating the dose falloff region in the proton therapy *Appl. Phys. Lett.* **89** 183517

Moskvin V, Cheng C W, Zhao Q and Das I J 2012 Comment on 'Comparison of secondary neutron dose in proton therapy resulting from the use of a tungsten alloy MLC or a brass collimator system' *Med. Phys.* **39** 2303–5

Moteabbed M, Espana A and Paganetti H 2011 Monte Carlo patient study on the comparison of prompt gammas and PET imaging for range verification in proton therapy *Phys. Med. Biol.* **56** 1063–82

Newhauser W, Fontenot J, Zheng Y, Polf J, Titt U, Koch N, Zhang X and Mohan R 2007 Monte-Carlo simulations for configuring and testing an analytical proton dose-calculation algorithm *Phys. Med. Biol.* **52** 4569–84

Nose H, Niita K, Hara M, Uematsu K, Azuma O, Miyauchi Y, Komori M and Kanai T 2005 Improvement of three-dimensional Monte Carlo code PHITS for heavy ion therapy *J. Nucl. Sci. Technol.* **42** 250–5

Paganetti H, Jiang H, Lee S Y and Kooy H M 2004 Accurate Monte Carlo simulations for nozzle design, commissioning and quality assurance for a proton radiation therapy facility *Med. Phys.* **31** 2107–18

Parodi K, Enghardt W and Haberer T 2002 In-beam PET measurements of $\beta+$ radioactivity induced by proton beams *Phys. Med. Biol.* **47** 21–36

Parodi K, Mairani A, Brons S, Hasch B G, Sommerer F, Naumann J, Jäkel O, Haberer T and Debus J 2012 Monte Carlo simulations to support start-up and treatment planning of scanned proton and carbon ion therapy at a synchrotron-based facility *Phys. Med. Biol.* **57** 3759–84

Parodi K, Paganetti H, Cascio E, Flanz J B, Bonab A A, Alpert N M, Lohmann K and Bortfeld T 2007a PET/CT imaging for treatment verification after proton therapy: a study with plastic phantoms and metallic implants *Med. Phys.* **34** 419–35

Parodi K, Pönisch F and Enghardt W 2005 Experimental study on the feasibility of in-beam PET for accurate monitoring of proton therapy *IEEE Trans. Nucl. Sci.* **52** 778–86

Parodi K *et al* 2007b Patient study on *in vivo* verification of beam delivery and range, using positron emission tomography and computed tomography imaging after proton therapy *Int. J. Radiat. Oncol. Biol. Phys.* **68** 920–34

PDG-Website 2012 http://pdg.lbl.gov/2012/reviews/rpp2012-rev-monte-carlo-numbering.pdf

Polf J C, Peterson S, McCleskey M, Roeder B T, Spiridon A, Beddar S and Trach L 2009 Measurement and calculation of characteristic prompt gamma ray spectra emitted during proton irradiation *Phys. Med. Biol.* **54** N519–27

Pshenichnov I, Mishustin I and Greiner W 2006 Distributions of positron-emitting nuclei in proton and carbon-ion therapy studied with Geant4 *Phys. Med. Biol.* **51** 6099–112

Richard M H *et al* 2011 Design guidelines for a double scattering Compton camera for prompt gamma imaging during ion beam therapy: a Monte-Carlo simulation study *IEEE Trans. Nucl. Sci.* **58** 87–94

Rinaldi I, Ferrari A, Mairani A, Paganetti H, Parodi K and Sala P R 2011 An integral test of FLUKA nuclear models with 160 MeV proton beams in multi-layer Faraday cups *Phys. Med. Biol.* **56** 4001–11

ROOT-Website 2012 http://root.cern.ch/

Seravalli E *et al* 2012 Monte Carlo calculations of positron emitter yields in proton radiotherapy *Phys. Med. Biol.* **57** 1659–73

Smeets J *et al* 2012 Prompt gamma imaging with a slit camera for real time range control in proton therapy *Phys. Med. Biol.* **57** 3371–405

Sommerer F 2007 Experiments and FLUKA simulations of ^{12}C and ^{16}O beams for therapy monitoring by means of in-beam positron emission tomography *PhD Thesis* CERN

Sommerer F, Cerutti F, Parodi K, Ferrari A, Enghardt W and Aiginger H 2009 In-beam PET monitoring of mono-energetic ^{16}O and ^{12}C beams: experiments and FLUKA simulations for homogeneous targets *Phys. Med. Biol.* **54** 3979–96

Sommerer F, Parodi K, Ferrari A, Poljanc K, Enghardt W and Aiginger H 2006 Investigating the accuracy of the FLUKA code for transport of therapeutic ion beams in matter *Phys. Med. Biol.* **51** 4385–98

Sorge H, Stöcker H and Greiner W 1989 Relativistic quantum molecular dynamics approach to nuclear collisions at ultrarelativistic energies *Nucl. Phys.* A **498** 567–76

Testa E, Bajard M, Chevallier M, Dauvergne D, Le Foulher F, Freud N, Létang J M, Poizat J C, Ray C and Testa M 2009 Dose profile monitoring with carbon ions by means of prompt-gamma measurements *Nucl. Instrum. Methods* B **267** 993–6

Zheng Y, Newhauser W, Fontenot J, Taddei P and Mohan R 2007 Monte Carlo study of neutron dose equivalent during passive scattering proton therapy *Phys. Med. Biol.* **52** 4481–96